Microelectronics Reliability 49 (2009) 544–550

Contents lists available at ScienceDirect

Microelectronics Reliability

journal homepage: www.elsevier.com/locate/microrel

Effect of bump size on current density and temperature distributions in flip-chip solder joints

Wei-Chih Kuan, S.W. Liang, Chih Chen *

Department of Materials Science and Engineering, National Chiao Tung University, Hsin-chu 30010, Taiwan, ROC

ARTICLE INFO

Article history:
Received 17 July 2008
Received in revised form 4 March 2009
Available online 2 April 2009

ABSTRACT

Three dimensional thermo-electrical analysis was employed to simulate the current density and temperature distributions for eutectic SnAg solder bumps with shrinkage bump sizes. It was found that the current crowding effects in the solder were reduced significantly for smaller solder joints. Hot-spot temperatures and thermal gradient were increased upon reducing the solder. The maximum temperature for solder joint with 144.7 μm bump height is 103.15 °C which is only 3.15 °C higher than the substrate temperature due to Joule heating effect. However, upon reducing the bump height to 28.9 μm, the maximum temperature in the solder increased to 181.26 °C. Serious Joule heating effect was found when the solder joints shrink. The higher Joule heating effect in smaller solder joints may be attributed to two reasons, first the increase in resistance of the Al trace, which is the main heating source. Second, the average and local current densities increased in smaller bumps, causing higher temperature increase in the smaller solder bumps.

1. Introduction

Recently, electromigration has been recognized as a critical reliability issue for flip-chip technology. The size of solder joint has been scaled down significantly in recent years and the amount of current carried by each bump has increased from 0.2 A to 0.4 A. The applied current for accelerated electromigration tests could be as high as 2 A [1]. Several studies investigate the electromigration behavior on different sizes of solder bumps. Liang et al. adopted the eutectic SnPb (e-SnPb) solder of about 150 μm height to study the electromigration phenomenon [2]. Ouyang et al. study the void formation during electromigration using 90 μm-high solder joints [3]. Chang et al. used Kelvin structure to monitor the change in resistance of 75 μm bump height during electromigration [4]. Moreover, electromigration in solder joints with bump size less than 30 μm is also investigated [5,6]. The volume effect of the solder joints on the reaction of intermetallic compound (IMC) is also examined. However, to our knowledge, not much work has been done on the current density and temperature distribution with the same layout but with different bump sizes. The current density and temperature in the solder bump would be the key factors to understand the electromigration behavior. In this study, we use finite-element method to obtain the results on the current density and temperature distributions with different bump sizes. Thus, this study throws more light on the effect of the shrinkage of the bump size on the current and temperature distributions.

2. Simulation

The simulation geometry used in this study is schematically shown in Fig. 1a. Throughout this text, it will be denoted as the 100% model. A thick-film under-bump-metallization (UBM) of 5 μm Cu was adopted on the chip side, and metallization of 5 μm electroless Ni was used on the substrate side. Eutectic SnAg solder was adopted for the bump materials. It is assumed that 1 μm Cu UBM was assumed to form 1.4 μm Cu_6Sn_5 IMC on the chip side. On the substrate side, we assumed that 0.5 μm Ni metallization was consumed and 1 μm Ni_3Sn_4 IMC was formed at the interface of the solder and the Ni metallization. Both Cu_6Sn_5 and Ni_3Sn_4 IMCs were assumed to be layered-type to avoid any difficulty that may arise during meshing process. The passivation and UBM openings were 85 and 120 μm in diameter, respectively. The metallization opening on the substrate was 144 μm in diameter. The bump height between the Cu UBM and Ni metallization was 144.7 μm. The dimension of the Al trace is 100 μm wide and 1.5 μm thick, whereas the Cu line on the substrate side is 80 μm wide and 25 μm thick. Since the Cu line is neither a major heat sink nor a major heat source, it is built only 50 μm long. The diameters of Al pad and Cu pad were 110 μm and 200 μm, respectively. Two solders with an Al trace were used in the simulation. The pitch was 400 μm. The above-mentioned dimension was defined as "Model 100%".

To investigate the bump size effect, the component dimensions of the model were scaled down to examine the change in current density and temperature. The diameter of the Al pad, the width of the Al trace and the Cu line, the radii of passivation opening,

* Corresponding author. Tel.: +886 3573 1814; fax: +886 3572 4727.
E-mail address: chih@mail.nctu.edu.tw (C. Chen).

0026-2714/$ - see front matter © 2009 Published by Elsevier Ltd.
doi:10.1016/j.microrel.2009.03.001

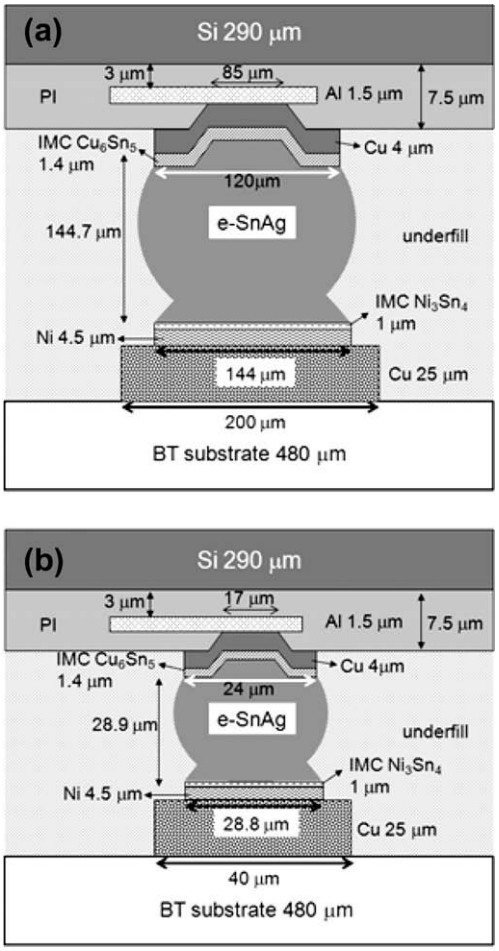

Fig. 1. The cross-sectional schematic models for the solder joints: (a) standard model which is denoted as the Model 100%, and (b) solder joint with dimensions reduced to 20% of the standard model, which is denoted as the Model 20%.

the UBM opening, and the metallization opening, the bump height, the diameter of Cu pad, and pitch of two solder joints were decreased proportionally to 80%, 60%, 40%, and 20%, respectively, of the standard model. Fig. 1b shows the schematic of "Model 20%". Therefore, the width of Al trace decreased from 100 μm to 20 μm. The passivation, UBM, and metallization openings become 17 μm, 24 μm, and 28.8 μm in diameter, respectively. The diameters of the Al pad and the Cu pad reduced to 22 μm and 40 μm, respectively. The width of Cu line has changed to 16 μm, the bump height has diminished to be 28.9 μm, and the pitch decreased down to 80 μm. However, the thicknesses of the Al trace, UBM layers, IMCs, and the Cu line remained the same as "Model 100%". More detailed information for the dimensions of all the models were listed in Table 1.

Table 2 lists the electrical resistivity, thermal conductivity, and temperature coefficient of resistivity (TCR) of the materials used in this simulation [7]. The effect of TCR was also considered in the simulation. A three dimensional (3D) simulation was carried out by finite-element analysis. After creating the volume model, the volume needs to be meshed for calculating the current density and temperature distributions. The meshing results for the "Model 100%" and "Model 20%" are shown in Fig. 2. To have a correct comparison with the bump size effect in simulation, a similar amount of elements need to be applied in different models. Thus, different element sizes occurred in different models. The average element size in "Model 100%" was about 3 μm. On the other hand, the average element size in "Model 20%" was about 0.6 μm to keep the same amount of elements.

Fig. 3 shows the constructed model for thermo-electrical simulation. Only two solder joints at the corner of the silicon were stressed by a current, as indicated by the arrow in Fig. 3. The dimension of the silicon die was 7.0 × 4.8 mm and its thickness was 290 μm, whereas the dimension of the bismaleimide triazine (BT) substrate was 5.4 mm wide, 9.0 mm long, and 480 μm thick. In addition, the dimensions of Si and BT would not be changed when the dimension of the solder joints was decreased. This is to maintain the same conditions of heat dissipation.

The 3D coupling thermo-electrical solid element analysis using ANSYS software was conducted to predict the steady-state temperature. The model used in this study was a SOLID69 eight-node hexahedral coupled field element. The thermo-electric was sequential. The field equations for the coupled thermo-electric analysis are:

$$\{q\} = T[\alpha]\{J\} - [K]\{\nabla T\} \quad (1)$$

$$\{J\} = [\sigma](\{E\} - [\alpha]\{\nabla T\}) \quad (2)$$

where Q is heat flux vector, T is absolute temperature, α is Seebeck matrix, J is electric current density, K is thermal conductivity matrix evaluated at zero current density, ∇T is thermal gradient, σ is electrical conductivity matrix evaluated at zero thermal gradient, and E is electric field.

For the thermal boundary conditions, the BT substrate was kept at 100 °C. Moreover, the convection parameter was in natural convection condition, whose heat convection coefficient in the air is usually between 5 W/m^2 °C and 15 W/m^2 °C. The ambient temperature and convection coefficient were taken as 25 °C and 10 W/m^2 °C. For the electrical boundary conditions, a constant current was applied through the left-hand side of Cu line in the substrate side. The voltage at the right-hand side of Cu end was set to be zero. The stressing currents ranged from 0.1 A to 0.5 A. A design space is being surveyed rather than that the designs studied represent possible products.

Table 1
The dimensions for the five simulation models in this study.

Unit (μm)	Model 100%	Model 80%	Model 60%	Model 40%	Model 20%
Diameter of Al pad	110	88	66	44	22
Width of Al trace	100	80	60	40	20
Pitch	400	320	240	160	80
Contact opening	85	68	51	34	17
UBM opening	120	96	72	48	24
Bump height	144.7	115.8	86.8	57.9	28.9
Metallization opening	144	115.2	86.4	57.6	28.8
Diameter of Cu pad	200	160	120	80	40
Width of Cu line	80	64	48	32	16

Table 2
The materials properties used in this paper.

Materials	Thermal conductivity (W/m K)	Resistivity (mΩ cm)	Temperature coefficient of resistivity (TCR) (K^{-1})
Al	238	2.7	4.2×10^{-3}
Al/Ni(V)Cu	166.6	29.54	5.6×10^{-3}
Cu_6Sn_5	34.1	17.5	4.5×10^{-3}
Pb–5Sn	63	19	4.2×10^{-3}
e-SnPb	50	14.6	4.4×10^{-3}
SnAg3.5	33	12.3	4.6×10^{-3}
Ni_3Sn_4	19.6	28.5	5.5×10^{-3}
Ni	76	6.8	6.8×10^{-3}
Cu	403	1.7	4.3×10^{-3}
Si	147	–	–
BT	0.7	–	–
Underfill	0.55	–	–
PI	0.34	–	–

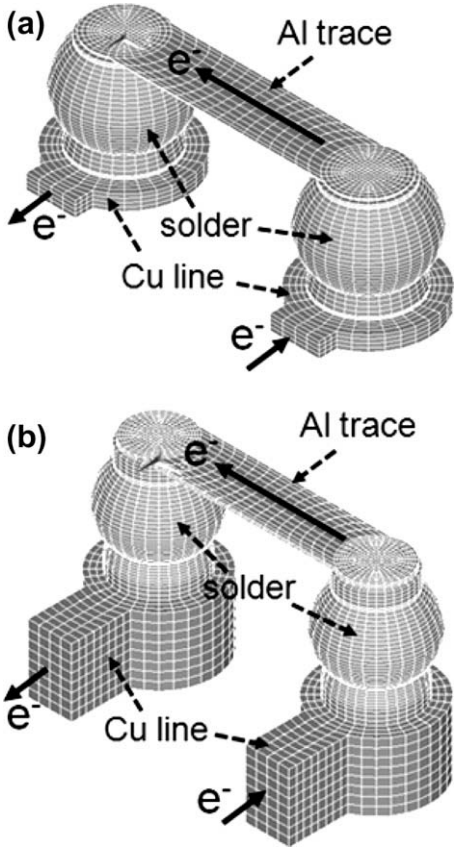

Fig. 2. Three dimensional view of the constructed model with meshization and the arrow shows the electric current flow: (a) the standard model, and (b) model 20%.

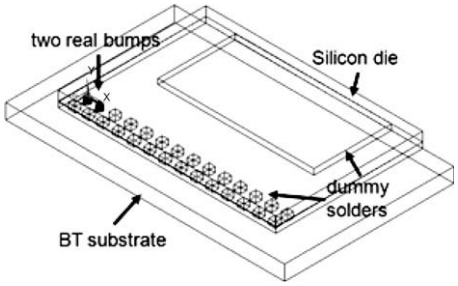

Fig. 3. Constructed flip-chip package for thermal simulation, in which only two of the solder joints were subjected to current stressing, as indicated by one of the arrows.

3. Results

3.1. 3D Current density distribution in flip-chip solder joints

Fig. 4a illustrates the cross-sectional current density distribution for Model 100% along the *Z*-axis in the solder joint under 0.5 A. The current crowded in a small region of the solder joint near the entrance of the Al trace. The maximum current density was 1.03×10^4 A/cm^2 in the top solder since the current density in the Al trace is as high as 4.49×10^5 A/cm^2. The current entered into the solder joint from the Al trace, and then drifted down vertically toward the substrate (along *Y*-axis), and also spread out laterally at the same time (along *X*-axis and *Z*-axis). Thus, the solder close to the entrance carried a high density of current. Fig. 4b–e shows the current density distributions for Model 80%, Model 60%, Model 40%, and Model 20%, respectively. As the solder shrank, the majority of the current still crowded into the UBM and solder joints. Especially, when the size of the solder bump decreased to 20%, high current density appeared over half of the UBM and larger regions in the solder bump. The maximum current density of Model 80%, Model 60%, Model 40%, and Model 20% are 1.45×10^4 A/cm^2, 2.38×10^4 A/cm^2, 4.68×10^4 A/cm^2, and 1.54×10^5 A/cm^2, respectively, when they are supplied by 0.5 A current. Fig. 5 summarizes the maximum current density as a function of UBM opening. Under the same applied current, the maximum current density is found to increase upon decreasing the UBM opening. The 20% model has the highest maximum current and it is about 15 times larger than that of 100% Model.

Fig. 6 shows the trend of crowding ratio for all the five models. The "crowding ratio" was denoted as the local maximum current density divided by the average current density on the UBM opening which was obtained by assuming a uniform current spreading on the UBM opening. The crowding ratio indicates the degree of unbalance in the current distribution in the solder bump. It is realized that the current crowding effect would accelerate the electromigration damage because of the enhanced wind force in the current crowding region. The average current densities on the UBM opening are 4.42×10^3 A/cm^2 in Model 100%, 6.91×10^3 A/cm^2 in Model 80%, 1.23×10^4 A/cm^2 in Model 60%, 2.76×10^4 A/cm^2 in Model 40%, 1.11×10^5 A/cm^2 in Model 20%. The crowding ratio inside the solder in Model 100% is about 2.3, which means that the local current density is 2.3 times larger than the average one on the UBM opening. Similarly, the crowding ratio is 2.1, 1.9, 1.7, and 1.4 for the Model 80%, 60%, 40%, and 20%, respectively. It is interesting that the crowding ratio in Model 20% is the smallest among the five models. This may be attributed to the fact that the Model 20% has small UBM opening for electric conduction. Most of the opening area is in the current crowded region. In addition, the average current density for the Model 20% is also higher than the

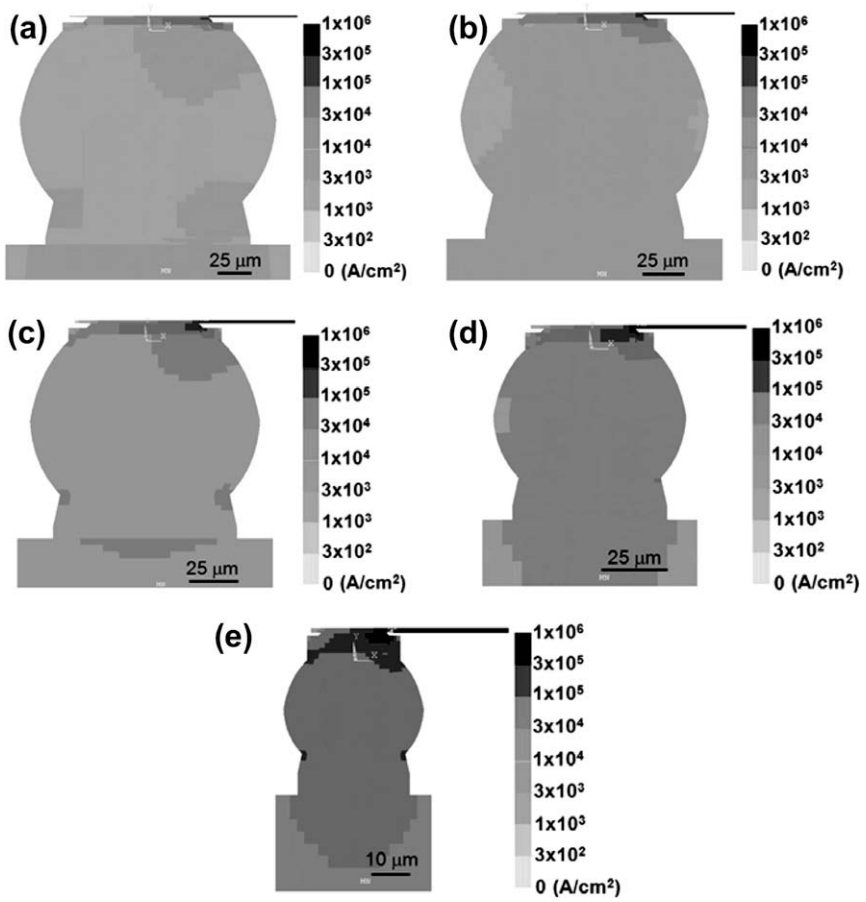

Fig. 4. Cross-sectional view of current density distribution in the solder joints for: (a) Model 100%, (b) Model 80%, (c) Model 60%, (d) Model 40%, and (e) Model 20% when a current of 0.5 A was applied.

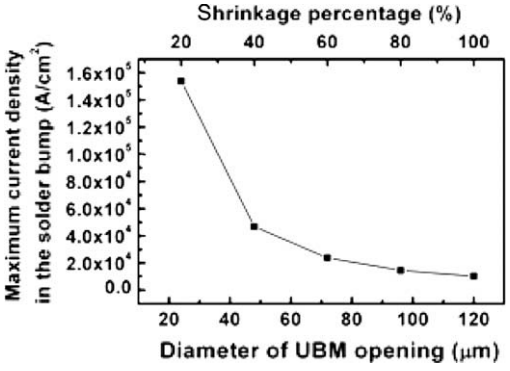

Fig. 5. Plot of maximum current density in the solder bump against the diameter of the UBM opening.

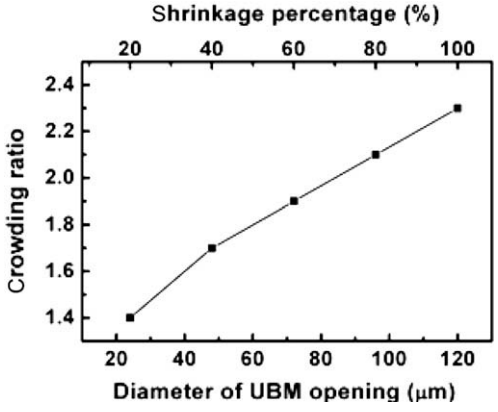

Fig. 6. Plot of crowding ratio against the diameter of the UBM opening.

rest of the models. Thus, the current crowding effect can be relieved by decreasing the bump size. However, it is noteworthy that both the average and the maximum current densities are higher in the smaller bump. Thus the smaller bumps will fail earlier.

3.2. 3D Temperature distribution in flip-chip solder joints

The dimension of the Al trace has significant effect on the Joule heating of solder bumps due to its large resistance. Fig. 7a–e shows the temperature distribution in the Al trace and in the solder bumps for the five models stressed by 0.5 A at 100 °C. It is found that the maximum temperature in the Al trace in Model 100% was 108.4 °C, whereas it increased to 202.1 °C in Model 20%. This is because both the width and length of the Al trace decreased upon reducing the joint size. Thus, the resistance of the Al trace was 71.3 Ω, 90.8 Ω, 92.3 Ω, 96.1 Ω, and 115.0 Ω for the five models. Since the heating power was equal to I^2R, the large Al trace resistance induced higher joule heating since the heat dissipation was almost the same. Fig. 8a–e illustrates the cross-sectional temperature distributions in the solder bump for the five models when they experienced an applied current of 0.5 A at 100 °C. A hot-spot inside the solder bump was observed near the entrance point of the Al trace by two reasons: First, the Al trace was the main heating

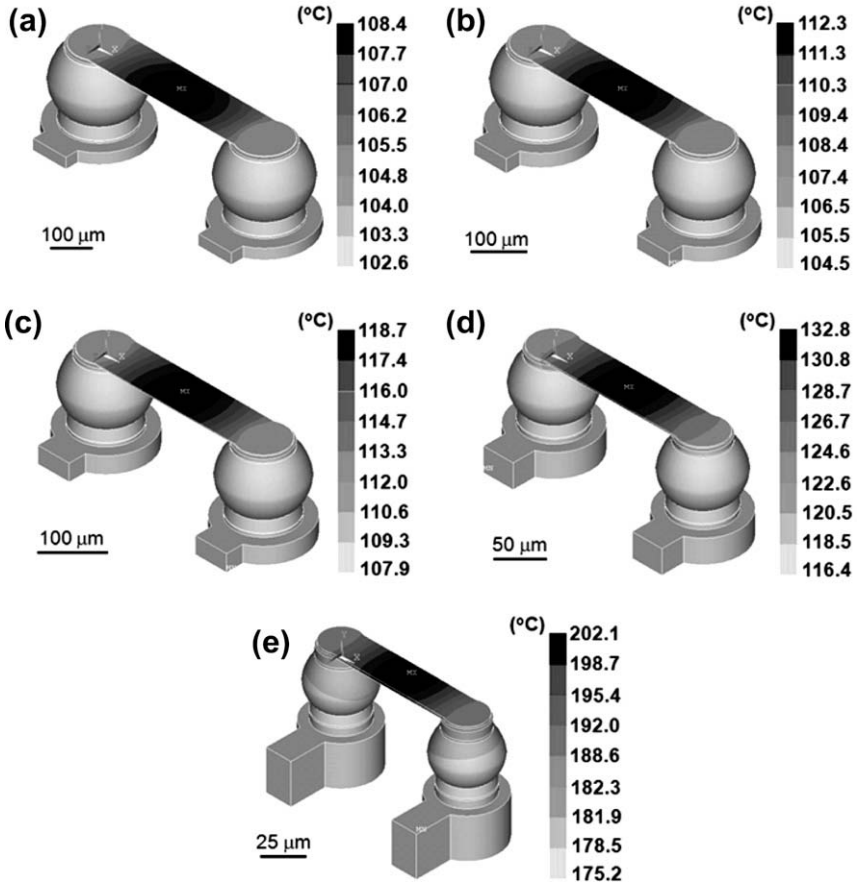

Fig. 7. The Joule heating effect in the solder joints for: (a) Model 100%, (b) Model 80%, (c) Model 60%, (d) Model 40%, and (e) Model 20% when a current of 0.5 A was applied on 100 °C substrate.

source. The generated heat dissipated into the solder directly. Second, the current crowding effect induced local joule heating effect in the solder bump near the entrance of the Al trace. The average temperature was obtained by averaging the node temperatures in the center of the solder. The temperatures in the hot-spot are 103.2 °C, 105.3 °C, 109.1 °C, 119.0 °C, and 181.3 °C, respectively, when the five models are stressed by 0.5 A, whereas the average temperatures were 102.9 °C, 104.8 °C, 108.4 °C, 117.6 °C, and 178.8 °C. A higher temperature increase was observed in smaller solder joules because of higher Joule heating of the reduced Al trace. Fig. 9a and b shows the hot-spot and average temperatures as a function of the applied current from 0.1 A to 0.5 A for the five models. At a lower stressing current of 0.1 A, the hot-spot and the average temperatures are almost the same. However, the temperature differs significantly at higher stressing currents. Model 20% has the highest increase in both hot-spot and average temperatures. For Model 100%, Model 80%, Model 60%, Model 40%, and Model 20%, the differences in temperature between hot-spot and average temperature are 0.3 °C, 0.5 °C, 0.7 °C, 1.4 °C, and 2.5 °C, respectively. For smaller solder joints, there is an increase temperature differences between the hot-spot and the average temperature.

Thermal gradient was built up across the solder bump due to the non-uniform temperature distribution. The thermal gradient was derived from the temperature difference between the hot-spot and the bottom of the solder on the substrate divided by the bump height. The thermal gradients for Model 100%, Model 80%, Model 60%, Model 40%, and Model 20% are 29 °C/cm, 82 °C/cm, 118 °C/cm, 340 °C/cm, and 1530 °C/cm as shown in Fig. 10. It can be observed that Model 20 exhibits the highest thermal gradient, which implies that as the solder becomes smaller, the thermomigration issue may become more critical.

4. Discussion

With the decrease in dimension of the solder joints, the increase in temperature and current density are related. The increase in temperature was defined as the temperature in the solder bump minus the substrate temperature, which was 100 °C. The increase in temperature in Model 20% is much more significant than the other models. Under the current stressing of 0.5 A, the increase in temperature for Model 20% is 81.3 °C at hot-spot, which is 25.4 times greater than Model 100%, whereas the area of UBM opening in Model 20% is 1/25 times smaller than Model 100%. Similarly, for Model 60%, the increase in temperature is 9.1 °C at hot-spot, which is 2.82 times greater than that for Model 100%, whereas the area of UBM opening in Model 60% is 1/2.78 times smaller than Model 100%. Fig. 11 shows the relationship between the increase in temperature and the inverse of UBM area with stressing current ranging from 0.1 A to 0.5 A. As shown in the figure, the relationship between the increase in temperature in the hot-spot and the inverse of passivation area is linear. It may indicate that serious Joule heating effect could take place upon decreasing the dimension of the solder joints.

To explain this phenomenon, Joule heating theory was used. In general, the Joule heating power can be expressed as:

$$P = I^2R = j^2\rho v \tag{3}$$

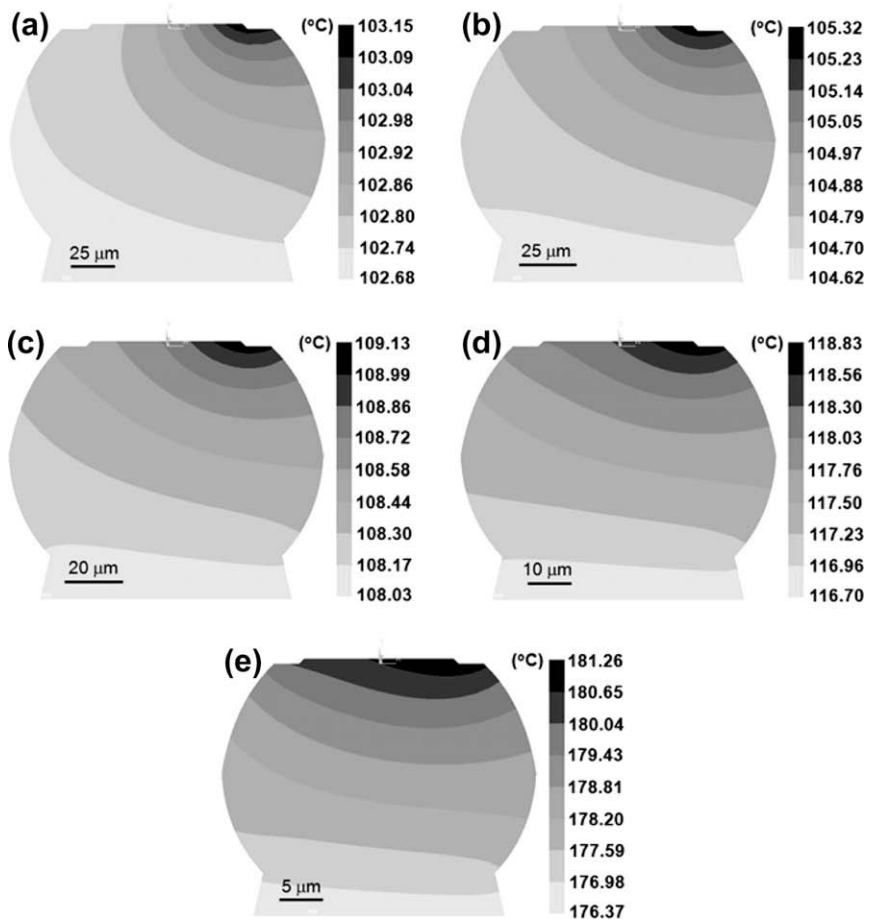

Fig. 8. Cross-sectional view of the temperature distribution in the solder bump for: (a) Model 100%, (b) Model 80%, (c) Model 60%, (d) Model 40%, and (e) Model 20% when a current of 0.5 A was applied and the substrate was kept at 100 °C. Only the solder bumps are shown.

where P is the Joule heating power, I is the current, R is the total resistance of the circuit, j is the local current density, ρ is the resistivity, and v is the local volume. As described above, the maximum current densities of Model 100%, Model 80%, Model 60%, Model 40%, and Model 20% are 1.03×10^4 A/cm^2, 1.45×10^4 A/cm^2, 2.38×10^4 A/cm^2, 4.68×10^4 A/cm^2, and 1.54×10^5 A/cm^2, respectively. It increased significantly upon decreasing the size of the bump. Thus, the local Joule heating becomes considerable at small bumps, resulting in a much higher hot-spot temperature. Therefore, the Joule heating effect would become larger at smaller solder joints because of the high resistance of the Al trace and the large local current density.

Furthermore, the hot-spot temperatures in solder bumps were obtained at various stressing temperatures for the five models. It is found that the hot-spot temperature was 107.8 °C upon stressing with 0.1 A for Model 20%, which is higher than 103.2 °C for the joints of Model 100% stressed by 0.5 A. The maximum current density of Model 20% stressed at 0.1 A is 3.1×10^4 A/cm^2, whereas it is 1.03×10^4 A/cm^2 for the Model 100%. If we assume that the failure mode and the activation energy are the same for the two stressing conditions, one could estimate the mean-time-to-failure (MTTF) using the equation for solder joints, which is typically expressed as [8]

$$\mathrm{MTTF} = A\frac{1}{j^n}\exp\frac{Q}{KT} \tag{4}$$

where A is a constant which contains a factor involving the cross-sectional area of the joint, j is the current density in amperes per centimeter square, n is a model parameter for current density, Q is the activation energy, k is Boltzmann's constant, and T is the average bump temperature in degrees Kelvin. It is noteworthy that this equation is proven valid for Al and Cu interconnects, but needs to be modified for application in solder joints. In this letter, the maximum current density and the hot-spot temperature were adopted for the values of j and T, respectively, to estimate the MTTF as voids form in the high current density and the hot-spot region. In addition, the values of n and Q used are 1.8 eV and 0.691 eV, respectively, for the SnPb solder with Ti/Ni(V)/Cu UBM structure [9,10]. It is noteworthy that n values could be much higher when joule heating is significant and, thus, it may influence the estimation of MTTF. We take the MTTF for Model 20% at 0.5 A as 1. Then the MTTF for all the five models stressed from 0.1 A to 0.5 A can be estimated. Table 3 summaries the MTTF ratios for all the simulated stressing conditions in this study. As one can see, the MTTF for the Model 20% at 0.1 A is still much shorter than that for Model 100% at 0.5 A, since both the hot-spot temperature and the maximum current density are larger in Model 20%. Therefore, the current carrying capability for smaller bumps decreases significantly. Furthermore, the analysis indicates that the higher maximum current density is the main contributor for shorter MTTF in a smaller bump stressed. For example, the MTTF for 100% model is 5063.1 times longer than the 20% model at 0.5 A, in which the current density effect contributes 130.2 times while the Joule heating effect contributes 38.9 times. Yet, for 40% and 20% models, the effect of Joule heating on MTTF becomes more significant than the current density effect. For 20% model stressed at 0.1 A, the MTTF is 545.0 times longer than the 20% model stressed at

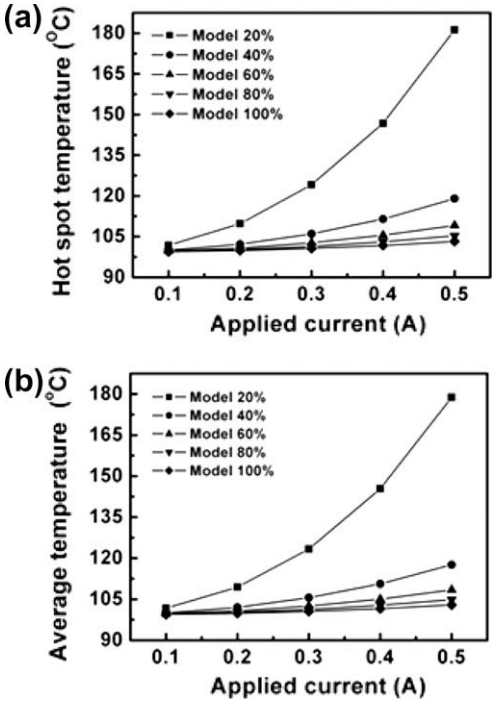

Fig. 9. (a) Hot-spot temperature as a function of the applied current for the five models. The hot-spot temperature increases as the bump size decreased and (b) average temperature in the solder as a function of the applied current for the five models. The average temperature increases as the bump size is decreased.

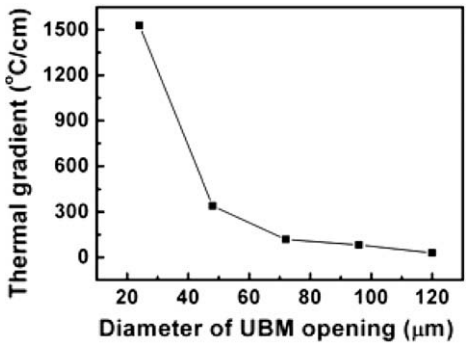

Fig. 10. Thermal gradient as a function of the UBM opening. Significant thermal gradients were established when the solder size decreased.

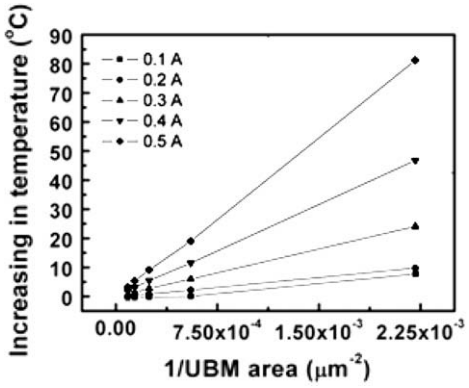

Fig. 11. The relationship between the temperature increase versus the inverse of UBM area with the applied current ranging from 0.1 A to 0.5 A.

Table 3
The MTTF ratio for the five models stressed at 0.1 A to 0.5 A. The MTTF for Model 20% at 0.51 A is set to 1.0.

Model (%)	Applied current (A)				
	0.1	0.2	0.3	0.4	0.5
100	114008.1	31809.3	14642.5	8239.1	5063.1
80	61245.2	16892.7	7600.7	4041.9	2430.6
60	24813.2	6688.9	2892.8	1472.0	807.0
40	7220.6	1828.2	711.3	313.2	140.7
20	545.0	140.2	31.8	6.4	1.0

0.5 A. In this case, the Joule heating effect contributes 30.1 times, whereas the current density effect only contributes 18.1 times. Therefore, Joule heating effect plays critical role on MTTF for very smaller bumps.

5. Conclusions

The current density and temperature distributions in flip-chip solder joints with several reduced bump sizes have been simulated by the finite-element method. The results revealed that as the solder joints became smaller, the solder bumps possessed a higher maximum current density and a higher hot-spot temperature. On the other hand, as the solder size is reduced, the crowding ratio is also decreased. Therefore, the electromigration would become a critical reliability issue as the solder joints continues to scale down. Also, the thermal gradient would become larger due to the higher carrier current density and higher Joule heating effect. Then, the thermo-migration issue would be another important issue in the future. The higher Joule heating effect in the smaller solder joints may be attributed to two reasons: first the increase in resistance of the Al trace, which was the main heating source. Second, the average and maximum current densities are higher for smaller bumps.

Acknowledgement

The authors would like to thank the National Science Council of ROC. for the financial support through Grant No. 95-2221-E-009-088-MY3.

References

[1] Tu KN. Recent advances on electromigration in very-large-scale-integration of interconnects. J Appl Phys 2003;94:5451.
[2] Liang SW, Chiu SH, Chen Chih. Effect of Al-trace degradation on Joule heating during electromigration in flip-chip solder joints. Appl Phys Lett 2007;90(8):082103.
[3] Ouyang F-Y, Tu KN, Lai Y-S, Gusak AM. Effect of entropy production on microstructure change in eutectic SnPb flip chip solder joints by thermomigration. Appl Phys Lett 2006;89(22):221906.
[4] Chang YW, Chiang TH, Chen Chih. Effect of void propagation on bump resistance due to electromigration in flip-chip solder joints using Kelvin structure. Appl Phys Lett 2007;91(13):132113.
[5] Chang YW, Liang SW, Chen Chih. Study of void formation due to electromigration in flip-chip solder joints using Kelvin bump probes. Appl Phys Lett 2006;89(3):032103.
[6] Yang D, Wu BY, Chan YC, Tu KN. Microstructural evolution and atomic transport by thermomigration in eutectic tin–lead flip chip solder joints. J Appl Phys 2007;102:043502.
[7] Chen Chih, Liang SW. Electromigration issues in lead-free solder joints. J Mater Sci: Mater Electron 2007;18(1):259–68.
[8] Black JR. IEEE Trans Electron Dev 1969;ED-16(4):338.
[9] Lai Y-S, Chen K-M, Kao C-L, Lee C-W, Chiu Y-T. Electromigration of Sn-37Pb and Sn–3Ag–1.5Cu/Sn–3Ag–0.5Cu composite flip-chip solder bumps with Ti/Ni(V)/Cu under bump metallurgy. Microelectron Reliab 2007;47(8):1273–9.
[10] Brandenburg S, Yeh S. Electromigration studies of flip chip solder bump solder joints. In: Proc of surface mount international conference and exhibition, San Jose; 1998. p. 337–44.